

Phase-Shimming of the BESSY II in-Vacuum APPLE II Undulator IVUE32 with Transverse Slides *

J. Bahrtdt ^{1 a)}, S. Grimmer ¹, M. Scheer ¹

¹ Helmholtz-Zentrum Berlin für Materialien und Energie, Wilhelm-Konrad-Röntgen-Campus, Albert-Einstein-Straße 15, 12489 Berlin, Germany

*) Work supported by ATHENA, a project of the Helmholtz Association.

a) johannes.bahrtdt@helmholtz-berlin.de

Abstract. The phase shimming of an in-vacuum APPLE II undulator requests a precise slit adjustment between neighbouring magnet rows besides the conventional gap tuning such as in an in-vacuum undulator. In an out-of-vacuum APPLE II, the slit between the magnet rows is precisely defined via a stiff needle bearing, which is located closely to the critical volume. In the APPLE II design, the slit adjustment must be done from outside of the vacuum chamber far away from the electron beam. In this article, we discuss the tolerances of systematic phase errors of various types and their relaxation with emittance and energy spread. We developed specific transverse slides for the slit adjustment to achieve full flexibility in phase tuning. We discuss their capability in slit adjustment precision in the readily assembled and evacuated system. The discussions are based on spectral and FEM-simulations.

1. Introduction

Two general trends determine the development of new undulator designs in modern synchrotron radiation facilities: i) pushing for shorter periods, smaller gap, and thus in-vacuum and cryogenically cooled devices; ii) achieving full polarization control. The combination of both technologies will be the next step. Existing in-vacuum devices at storage rings do not provide this flexibility. At HZB/BESSY II, two experiments demand for such a device: i) a soft X-ray microscope will cover the 4f-shells up to 2000 eV and the sulfur edge at around 2500eV with arbitrary polarization; ii) a RIXS-experiment will utilize the vertical polarization mode, which has only a minor angular dependence. Generally, above 3000 keV circularly polarized light can be produced from a planar undulator radiation via a quarter wave plate. In the soft X-ray regime, however, a variably polarizing undulator is the only choice.

At HZB/BESSY II the in-vacuum APPLE II undulator IVUE32 with a period length of 32mm is under construction [1]. The complete motion control system is placed in air, and thus, standard components for motors, gear boxes, screws, bearings and encoders can be utilized. The reduced stiffness of the magnet structure is alleviated with a new force compensation system [2]. The magnet gluing of BESSY II undulators is replaced with a UHV-compatible soldering technique. The gap and shift motion are measured from the outside via optical micrometers. This is an extension of a new measurement principle, which was implemented successfully in the cryogenic undulator CPMU17 at BESSY II [3]. The IVUE32 is the first step towards an in-vacuum cryogenically cooled APPLE with a period length of roughly 15mm [4].

One might think that the combination of two well-established technologies, in-vacuum undulators including CPMUs and APPLE II devices in a single device is a straight forward procedure, however, several additional new issues have to be solved.



This article concentrates on the systematic phase errors in an in-vacuum APPLE II and on methods for an efficient shimming. The random phase errors will be removed already via a magnet sorting procedure, as has been done successfully for numerous in-air APPLE II at BESSY II. Conventional planar undulators are shimmed to final precision at an in-air Hallprobe bench. The installation into the vacuum tank may introduce systematic gap errors which produce systematic phase errors. Usually, these errors are compensated with tapering the magnet girders and a mechanic length adjustment of the vertical columns, which support the in-vacuum magnet girders. A compact in-vacuum measurement bench is needed for the spectral tuning and qualification of the device. A gap variation within 20 μ m was achieved at the CPMU17 already without mechanic shims. An in-vacuum APPLE II employs another sensitive degree of freedom, the slit between neighboring magnet rows. For the slit adjustment dedicated tools, i.e.: transverse slides will be used. This strategy will be presented in this paper.

2. Systematic Phase Errors

The IVUE32 will cover the Sulfur edge at 2472 eV with the 7th harmonic. The acceptable loss of on-axis flux density at the 7th harmonic due to field errors is specified to be $I_r^7/I_0^7 \leq 10\%$. The reduction for zero emittance and zero energy spread was derived by Walker [5], $Re = I_r^n/I_r^0 = \exp(-(n \cdot \sigma_\phi)^2)$, with n =undulator harmonic and σ_ϕ = phase error. The phase error is evaluated at the extrema, i.e.: the location where the radiation is generated. Walker demonstrated numerically the relaxation of phase error specifications with the inclusion of emittance and energy spread [6]. Only recently, Tanaka presented an analytic model for the evaluation of the reduction factors including the electron beam properties and the beamline acceptance [7]. In this paper we utilize the numeric code WAVE [8] for the evaluation of the on-axis flux density including emittance and energy spread. We study solely the combined effect of systematic phase errors and electron beam properties on the reduction factors. For a better understanding we skip the random phase errors at this point. In [6] Walker studies real devices where random errors and systematic errors both are present.

Within the design phase a thorough evaluation of random and systematic phase error sources is crucial (e.g.: [9]). Usually, residual random errors are shimmed, whereas systematic errors have to be regarded already in the design phase. In [10], the phase errors of various systematic, periodic errors of the European XFEL undulators are evaluated analytically (straight trajectories are assumed). Later [11], the formalism was complemented with the shape of a quadratic girder bending. The phase errors are derived from the field errors as follows, left [10], right [11]:

$$\sigma_\phi = \alpha \frac{4\pi}{\lambda_u} \frac{K_0^2}{1+K_0^2} \frac{\Delta K_0}{K_0} \Big|_{\substack{\Delta K_0= \\ 0.5 \cdot \text{full range}}} \cdot \lambda_\delta \qquad \sigma_\phi = \alpha \frac{4\pi}{\lambda_u} \frac{1}{1+2/K^2} \frac{\Delta K}{K} \Big|_{\substack{\Delta K= \\ \text{full range}}} \cdot \lambda_\delta$$

The expressions in [10] and [11] are equivalent, though the variables are slightly different. In [11], K is the maximum value (in [10] K_0 is the rms-value), λ_δ is the length of the undulator (length of the error period in [10]) and ΔK is the total max-min variation of K (the amplitude of the periodic variation in [10]). λ_u is the undulator period and α is a constant, which describes the geometric shape of a specific error. α is derived analytically for periodic systematic errors of sinusoidal, sawtooth (including taper), triangular, constant and parabolic shape [10] and for a non-periodic quadratic bending error [11]. Within this paper we derived analytically also the α -values for a 3rd-order and 4th-order bending (following [11]) and for a cosine (following [10]). All coefficients α are summarized in **Table 1**. The analytic form of the phase error above illustrates the linear scaling with the error extension, λ_δ . Thus, it is more efficient to correct for the long-range errors rather than for the shorter ones. The errors scale non-linearly with the period length and the undulator strength K and linearly with the shape of the distortion (linear in α).

The phase errors in the 2nd-last column of **Table 1** are evaluated for the field errors in columns one and two at smallest gap of 7mm and with a relative strength of $\Delta K_0/K_0 = 0.003$ ($\Delta K/K = 0.006$). In all cases a regression line has been subtracted for a minimization of the phase error. The phase errors employ either mirror symmetry or point symmetry. In the first case, the regression line is solely an offset, and in the latter case, a straight line through the origin, which causes a detuning of the resonance

energy. Though equal in strength, the field errors yield phase errors over a wide range. **Figure 1** shows the six corrected phase errors with phase errors as listed in the 2nd-last column of **Table 1**.

Table 1. Systematic phase errors and the relevant α -values for the IVUE32. The last two columns give the phase errors at the 7th harmonic at the smallest gap (7mm) and at 2500eV as derived numerically with the HZB-code ANALYZE (dedicated to the analysis of ID-fields). The analytic values and the reference to the corresponding equation are given in brackets (2nd last column).

Error Function	α	Reference to α	σ_φ (7mm gap)	σ_φ (2500eV)
sine	$(1/2\pi) \cdot \sqrt{1/2}$	[10]	15.44° (15.55° [10])	11.17°
cosine	$(1/2\pi) \cdot \sqrt{1/2 - 3/\pi^2}$	this paper	9.51° (9.74° [10])	6.88°
taper	$1/(6 \cdot \sqrt{5})$	[10]	10.03° (10.30° [10])	7.26°
bending	$1/\sqrt{1575}$	[11]	6.67° (6.96° [11])	4.82°
3 rd order	1/60	this paper	4.37° (4.61° [11])	3.16°
4 th order	$2/\sqrt{13475}$	this paper	4.46° (4.76° [11])	3.23°

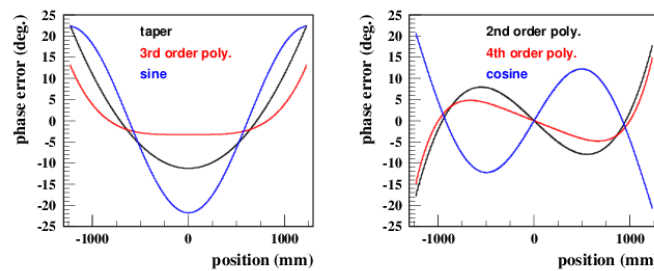


Figure 1. Phase errors of mirror symmetry (left) and point symmetry (right) phase errors, corresponding to last column of **Table 1**.

Figure 2 shows the 7th harmonic at 2500eV including the phase errors of **Table 1**, last column. A detuning and reshuffling of intensity from the main lobe into the side lobes is observed, and in some cases the main lobe disappears (sine error). The single electron spectra (red) depend upon the error symmetry. The symmetry of the fine structure remains more prominent for point symmetric field errors (taper, sine) than for mirror symmetric field errors (e.g.: bending, cosine). Though the emittance reduces the intensity by roughly an order of magnitude, the fine structure is pretty much preserved. Differently, the energy spread reduces the intensity only by a factor of two, but it completely washes out the fine structure. This is because the emittance redistributes the intensity mainly in the solid angle, whereas the energy spread solely acts on the energy axis. In consequence, the spectral sensitivity on phase errors is strongly alleviated with energy spread, as long as the fine structure distribution is hidden under the energy spread footprint (blue curve). In contrast, even with emittance the spectral sensitivity on phase errors is still high, as long as the fine structure is visible.

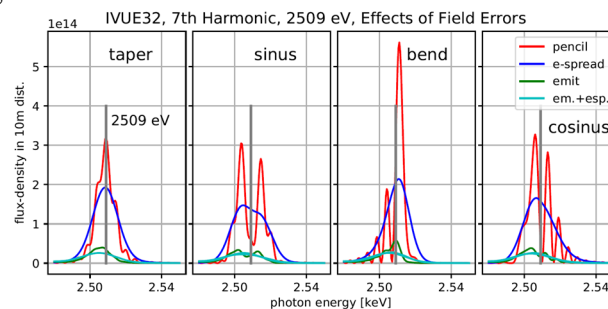


Figure 2. Spectral properties of the IVUE32, with mirror symmetric (1st, 2nd graph) and point symmetric (3rd and 4th picture) phase errors (**Table 1**, last column) with & without (pencil) emittance & energy spread included.

3. On-Axis Flux Density Reduction from Systematic Phase Errors Including e-Beam

The main lobe or side lobe with the highest intensity depends upon the phase error type and the strength. No analytic approach for a prediction of the impact of these specific errors on the spectral performance is available. Thus, we investigated the on-axis flux density reduction due to systematic field / phase errors including emittance and energy spread numerically (WAVE) for the six error types in **Table 1 (Figure 3)**. The single electron values follow closely Walker's derivation, though our systematic phase errors are not Gaussian distributed. This is explained within the Central Limit Theorem (CLT): Even if the population distribution of the electric field components of the amplitudes from the individual poles are non-Gaussian, the sample distribution approaches a normal distribution for larger sums, which is usually the case for undulators [5]. Larger deviations occur only above $n \cdot \sigma_\phi \approx 1.0$ (rad). Here, the intensity starts to get reshuffled from the main lobe to the side lobes, which cannot be described analytically. As mentioned already, the emittance has a stronger impact on the reduction factors than the energy spread. The sine and taper errors have the biggest influence on the reduction factors, if emittance and energy spread are included. The taper will not be discussed here, because it can (and must) always be corrected for. Therefore, we concentrate on the sine error (2500eV): A reduction of 10% (20%) requests for the following phase errors: BESSY II: $\sigma_\phi = 4,9^\circ$ ($8,2^\circ$), DLSR (only energy spread): $\sigma_\phi = 4,1^\circ$ ($6,1^\circ$). For comparison the values for a single electron (Walker [5]): $\sigma_\phi = 2,6^\circ$ ($3,8^\circ$).

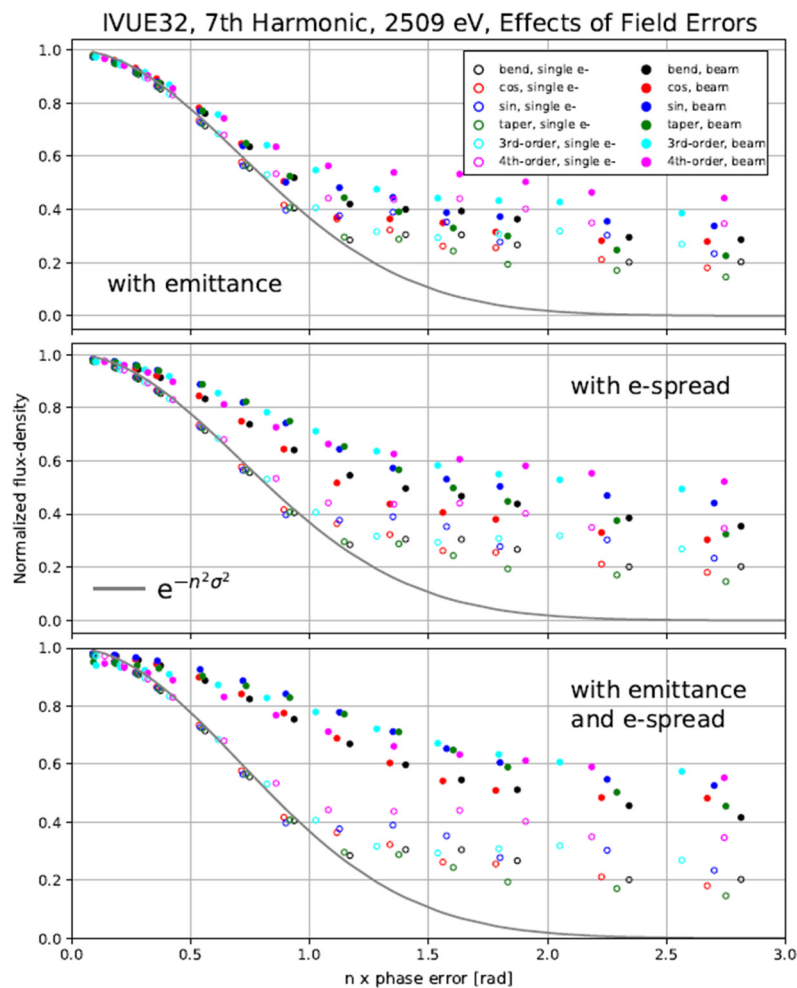


Figure 3. Numeric simulations with WAVE with emittance and energy spread of BESSY II. Top: On-axis flux density reduction dependent upon phase error strength of the IVUE32 without (open circles) and with (full circles) emittance, energy spread is zero. Center: Reduction with energy spread, emittance is zero. Bottom: Reduction with emittance and energy spread.

4. Strategy of systematic phase errors minimization

The magnetic field response of a transverse magnet row displacement at smallest gap is depicted in **Figure 4**. This is compared to the field integral response of a magnet keeper movement (virtual shim). In case of a virtual shimming, a horizontal / vertical keeper movement generates purely a vertical / horizontal field integral change. In contrast, for fields a decoupling is given only for a horizontal movement. A vertical magnet row displacement affects both field components (**Figure 4**). Thus, we decided to aim for a vertical gap homogeneity of $20\mu\text{m}$ via tight fabrication tolerances and precise assembly, which has been proven to be possible with the BESSY II-CPMU17. The horizontal and vertical field changes due to vertical displacement in the IVUE32 are: $-2.28\text{mT}/0.1\text{mm}$ and $-2.71\text{mT}/0.1\text{mm}$. The vertical gap will be checked via optical methods without chamber, and if necessary, it will be corrected. No changes with installation into the chamber are expected. This is different for the homogeneity of the slit between the magnet rows, which certainly will change during final assembly into the chamber. The slit width fluctuations will have to be corrected in-situ based on magnetic measurements. The horizontal and vertical field changes due to a horizontal displacement are $-0.13\text{mT}/0.1\text{mm}$ and $-2.30\text{mT}/0.1\text{mm}$. The tolerable phase error of the strongest error type (sine) corresponds to horizontal displacements of: BESSY II: $\Delta_z = -32\mu\text{m}$ ($-54\mu\text{m}$), DLSR (only energy spread): $\Delta_z = -27\mu\text{m}$ ($40\mu\text{m}$). Thus, we aim for an adjustment accuracy of $\Delta z \leq 30\mu\text{m}$, which yields a maximum on-axis flux density reduction of only 10% for a sine error. The slide settings will be controlled with adjustment plates being ground to the desired thickness.

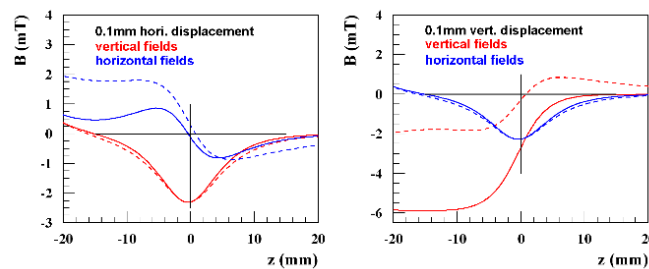


Figure 4. Magnetic field response of a transverse magnet row movement (solid lines) at 2500eV: left / right: horizontal / vertical slide displacement. For comparison field integral changes by virtual shims (dashed lines, in arbitrary units).

The shimming of the vertical fields is achieved via a horizontal displacement of two diagonal rows. There are two independent diagonal magnet rows, which are interlaced with respect to each other. Thus, using both pairs of magnet rows sine or cosine like errors can be compensated in amplitude and phase.

5. FEM-Simulations of Magnet Row Bending via Transverse Slide Displacement

A 2nd, 3rd and 4th order bending of a single magnet row is simulated, where the five individual slides define the shape with maximum displacements of 0.1, 0.2, and 0.3mm. The response of the magnets (**Figure 5**, left) follows closely this shape for the 2nd and 3rd order, whereas for the 4th order the amplitude is smaller and the shape is distorted. The shape can be symmetrized (dashed red curve) with a different displacement of column 4: 0.22mm instead of 0.30mm. The deformations show a common offset of several 0.1 mm, which is not real. It relates to specific boundary conditions in the FEM code, which permit the slide movement in the model. In the future the model will be refined to avoid this artificial offset. An incremental bending from 0.1 to 0.2mm and from 0.2 to 0.3mm demonstrates the linear reaction of the system at low orders, only at 4th order a non-linearity of a few percent shows up (**Figure 5**, center). This translates into a good predictability, which permits a fast iteration during shimming. The crosstalk into the orthogonal direction (vertical) amounts to only a few percent (**Figure 5**, right), and it increases with the bending order. This guarantees, that the gap homogeneity must be re-adjusted only at the first horizontal adjustment iteration, if at all. The iterations can be confined to the horizontal plane, which simplifies the whole procedure. The high frequency oscillations are attributed to numeric noise, which will be reduced in the future with optimized FEM-parameters.

The magnet row deformation introduces additional stress in the system. All critical parts such as the bolts of the columns, that support the rows, were checked carefully. They have a safety margin of at least a factor of 1.5 (grade A4-80) under all conditions if the deformations are restricted to 0.3, 0.2 and 0.1 mm for a 2nd, 3rd and 4th order bending. These limits can be extended with bolts of higher grade.

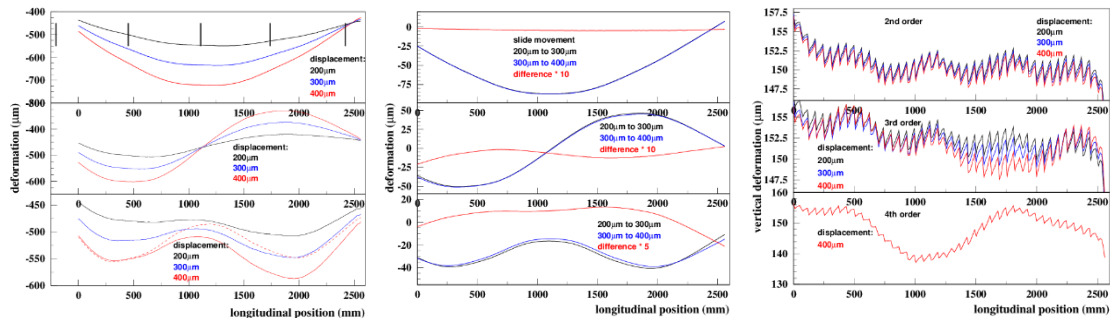


Figure 5. Results from FEM simulations for combined slide movements of 2nd, 3rd and 4th order shape. The response of the magnets is plotted. Top, center, bottom: 2nd, 3rd, 4th order. Left: displacement of magnets; center: linearity; right: crosstalk into the vertical plane. The position of the columns 1-5 (left to right) is indicated in the left graph, top with vertical bars.

6. Conclusion

We have studied the influence of several systematic phase errors of different characteristics on the spectral performance of the IVUE32. In reality, a combination of these errors will be present. They can be corrected to the tolerances via a displacement of the in-vacuum magnet girders under vacuum.

References

- [1] J. Bahrtdt et al., “IN-VACUUM APPLE II UNDULATOR,” Proc. IPAC 2018, Vancouver BC, Canada, pp. 4114-4116, 2018.
- [2] J. Bahrtdt and S. Grimmer, “In-vacuum APPLE II undulator with force compensation,” AIP Conference Proceedings, no. 2054, pp. 030031-1-6, 2019. A reference
- [3] J. Bahrtdt and E. Gluskin, “Cryogenic permanent magnet and superconducting undulators,” Nucl. Instrum. Methods Phys. Res. Sect. A, vol. 907, pp. 149-168, 2018.
- [4] E. Rial et al., “Cryogenically cooled in-vacuum APPLE,” these proceedings, 2022.
- [5] R. Walker, “Interference effects in undulator and wiggler radiation sources,” Nucl. Instrum. Methods in Phys. Res. A, vol. 335, pp. 328-337, 1993.
- [6] R. Walker, “Phase errors and their effect on undulator radiation properties,” PHYSICAL REVIEW SPECIAL TOPICS - ACCELERATORS AND BEAMS, vol. 16, pp. 010704-1-16, 2013.
- [7] T. Tanaka, “Universal representation of undulator phase errors,” PHYSICAL REVIEW SPECIAL TOPICS - ACCELERATORS AND BEAMS, vol. 21, pp. 110704 -1-16, 2018.
- [8] M. Scheer, “WAVE - A Computer Code for the Tracking of Electrons through Magnetic Fields and the Calculation of Spontaneous Synchrotron Radiation,” Proc. ICAP, Rostock-Warnemünde, Germany, pp. 86-88, 2012.
- [9] J. Bahrtdt and Y. Ivanyushenkov, “EFFECTS OF GEOMETRICAL ERRORS ON THE FIELD QUALITY IN A PLANAR SUPERCONDUCTING UNDULATOR,” Proc. of IPAC, New Orleans, LA, USA, pp. 708-710, 2012.
- [10] Y. Li, B. Faatz and J. Pflueger, “Undulator system tolerance analysis for the European x-ray free-electron laser,” PHYSICAL REVIEW SPECIAL TOPICS - ACCELERATORS AND BEAMS, vol. 11, pp. 100701-1-8, 2008.
- [11] Y. Li, B. Ketenglu and J. Pflueger, “Girder deformation related phase errors on the undulators for the European X-Ray Free Electron Laser,” PHYSICAL REVIEW SPECIAL TOPICS - ACCELERATORS AND BEAMS, vol. 18, pp. 060704-1-9, 2015.